A feasibility study: Selection of a personalized radiotherapy fractionation schedule using spatiotemporal optimization

Minsun Kim[a] and Robert D. Stewart
Department of Radiation Oncology, University of Washington, Seattle, Washington 98195-6043

Mark H. Phillips
Departments of Radiation Oncology and Neurological Surgery, University of Washington, Seattle, Washington 98195-6043

(Received 30 June 2015; revised 30 September 2015; accepted for publication 10 October 2015; published 26 October 2015)

Purpose: To investigate the impact of using spatiotemporal optimization, i.e., intensity-modulated spatial optimization followed by fractionation schedule optimization, to select the patient-specific fractionation schedule that maximizes the tumor biologically equivalent dose (BED) under dose constraints for multiple organs-at-risk (OARs).
Methods: Spatiotemporal optimization was applied to a variety of lung tumors in a phantom geometry using a range of tumor sizes and locations. The optimal fractionation schedule for a patient using the linear-quadratic cell survival model depends on the tumor and OAR sensitivity to fraction size (α/β), the effective tumor doubling time (T_d), and the size and location of tumor target relative to one or more OARs (dose distribution). The authors used a spatiotemporal optimization method to identify the optimal number of fractions N that maximizes the 3D tumor BED distribution for 16 lung phantom cases. The selection of the optimal fractionation schedule used equivalent (30-fraction) OAR constraints for the heart ($D_{\text{mean}} \leq 45$ Gy), lungs ($D_{\text{mean}} \leq 20$ Gy), cord ($D_{\max} \leq 45$ Gy), esophagus ($D_{\max} \leq 63$ Gy), and unspecified tissues ($D_{05} \leq 60$ Gy). To assess plan quality, the authors compared the minimum, mean, maximum, and D_{95} of tumor BED, as well as the equivalent uniform dose (EUD) for optimized plans to conventional intensity-modulated radiation therapy plans prescribing 60 Gy in 30 fractions. A sensitivity analysis was performed to assess the effects of T_d (3–100 days), tumor lag-time ($T_k = 0$–10 days), and the size of tumors on optimal fractionation schedule.
Results: Using an α/β ratio of 10 Gy, the average values of tumor max, min, mean BED, and D_{95} were up to 19%, 21%, 20%, and 19% larger than those from conventional prescription, depending on T_d and T_k used. Tumor EUD was up to 17% larger than the conventional prescription. For fast proliferating tumors with T_d less than 10 days, there was no significant increase in tumor BED but the treatment course could be shortened without a loss in tumor BED. The improvement in the tumor mean BED was more pronounced with smaller tumors (p-value = 0.08).
Conclusions: Spatiotemporal optimization of patient plans has the potential to significantly improve local tumor control (larger BED/EUD) of patients with a favorable geometry, such as smaller tumors with larger distances between the tumor target and nearby OAR. In patients with a less favorable geometry and for fast growing tumors, plans optimized using spatiotemporal optimization and conventional (spatial-only) optimization are equivalent (negligible differences in tumor BED/EUD). However, spatiotemporal optimization yields shorter treatment courses than conventional spatial-only optimization. Personalized, spatiotemporal optimization of treatment schedules can increase patient convenience and help with the efficient allocation of clinical resources. Spatiotemporal optimization can also help identify a subset of patients that might benefit from nonconventional (large dose per fraction) treatments that are ineligible for the current practice of stereotactic body radiation therapy.
 [http://dx.doi.org/10.1118/1.4934369]

Key words: fractionation schedule optimization, treatment planning, IMRT, optimization

1. INTRODUCTION

In radiation treatment planning, it is imperative to deliver a dose distribution that is highly conformal to the tumor, avoids critical normal structures, and is optimally fractionated in order to maximize the therapeutic ratio(s). Intensity-modulated radiation therapy (IMRT) emphasizes the spatial localization of dose by optimizing a fluence map for a given, predetermined fractionation schedule. Optimization of the fractionation schedule seeks the total number of fractions and the corresponding dose per fraction that maximize the biologically effective dose (BED) of the tumor while keeping the organ-at-risk (OAR) BED fixed (at acceptable limits). BED is the total physical dose corrected for the biological effect of a particular fractionation schedule using the linear-quadratic (LQ) cell survival model. While IMRT focuses on the spatial

distribution of a physical total dose, fractionation schedule optimization takes the biological impact of the dose distribution over time into account when assessing plan quality.

Fractionation schedule optimization using the LQ model was first proposed by Fowler in 1990s.[1,2] BED is a function of the total dose, the number of fractions (N), and tissue-specific radiosensitivity parameters (α/β). A basic model for spatiotemporal optimization incorporates one tumor, one OAR, and a scalar dose that is assigned to the tumor and OAR, rather than the actual dose distribution calculated in a patient-specific geometry of the tumor and OAR. An idealized model such as this facilitates an analytical solution and provides valuable insights into the optimal fractionation schedule problem, i.e., whether a short or long treatment course is beneficial for a specific type of tumor depending on the α/β ratio. Variations of the basic model have been investigated: Yang and Xing extended the LQ model to include the reoxygenation and redistribution of the tumor and used up to two OARs, but the solution was found using simulated annealing without the guarantee of optimality.[3] Another study by Bertuzzi *et al.* using up to two OARs had a fixed number of N in their model.[4] While the original model had the same dose to tumor and OAR, Mizuta *et al.* employed a sparing factor ($0 < s \leq 1$) such that the dose to OAR equals a fraction of the dose to tumor, i.e., $d_{\text{OAR}} = s d_{\text{tumor}}$, thereby acknowledging that d_{OAR} is often lower than d_{tumor}.[5] Unkelbach *et al.* used a heterogeneous dose distribution for a single OAR and introduced the effective sparing factor s_{eff} to relate the OAR dose to the tumor dose by $d_{\text{OAR}} = s_{\text{eff}} d_{\text{tumor}}$.[6] Bortfeld *et al.* studied the effect of accelerated tumor repopulation on the optimal fractionation schedule with a modification to the basic model.[7]

The conclusions from the previous studies were similar in essence: the analytical solution to the basic problem and the related variations depends on the difference in (i) the α/β ratios of the tumor and OAR and (ii) the relative dose received by them (s_{eff}). More specifically, if the α/β ratio of the tumor is equal to or less than the α/β ratio of OAR divided by the (effective) sparing factor, then a single fraction is optimal. Otherwise, an infinite number of fractions are optimal when the effective tumor doubling time is large compared to the overall treatment time, e.g., slowly proliferating tumor.

However, in modern radiotherapy, there are often multiple OARs competing with tumor coverage and consequently, the relationship between tumor dose and OAR dose cannot be unambiguously defined by a single parameter. Furthermore, the advances of IMRT have resulted in a highly heterogeneous dose distribution to maximize the tumor coverage and normal tissue sparing; therefore, the assumption of assigning a scalar dose to the tumor and OAR can lead to a suboptimal solution. Our previous publication in Ref. 8 explicitly addressed these concerns by proposing a model using a fluence map generated by standard methods for IMRT inverse planning as an input to fractionation schedule optimization. Using an actual heterogeneous dose distribution from IMRT, our model was able to incorporate three common types of constraints for OAR, namely, maximum dose, mean dose, and dose–volume histogram constraints for any number of OARs. The optimality of the solution was rigorously proven by mathematical analysis.

In current practice, nonconventional fractionation schedules are limited to stereotactic body radiation therapy (SBRT) with small tumors only. The purpose of this study is to investigate the feasibility of personalizing fractionation schedules for lung cancer patients using our previously published model in Ref. 8 and to assess the potential dosimetric benefits for a range of tumor sizes and locations. This work was motivated by the fact that relative doses between the tumor and OAR may vary significantly from one patient to another, resulting in the differences in the optimal fractionation schedule among patients. Plans using conventional prescription and spatiotemporal optimization were compared for 16 different anatomical combinations of a lung tumor and adjacent normal tissue structures (cord, esophagus, heart, right lung, and left lung) positioned within a representative thoracic phantom. All plans were optimized with the BED to OAR being constrained by equivalent tolerance doses. The potential impact of conventional and spatiotemporally optimized plans on local tumor control was assessed in terms of the tumor BED and equivalent uniform dose (EUD).

The paper is organized as follows: Sec. 2.A discusses the optimization models and solution methods used, followed by how the phantom studies were generated and planned in Sec. 2.B. Section 2.C presents how the quality of plan was assessed in this study. Finally, the comparison of plans using the conventional fractionation and spatiotemporally optimized fractionation is presented in Sec. 3, followed by the discussion in Sec. 4.

2. MATERIALS AND METHODS

In the basic model used in the previous studies surveyed in Sec. 1, a fractionation schedule is optimized to maximize the tumor BED by varying the total number of fractions (N) while fixing OAR BED to a constant regardless of N chosen,

$$\max_N \alpha^\tau N d + \beta^\tau N d^2 - \ln 2\,(T/T_d) \tag{1}$$
$$\text{subject to } \alpha^\phi N d + \beta^\phi N d^2 = \text{constant},$$

where

τ : tumor, ϕ : OAR,
α, β : tissue-specific radiosensitivity parameters in the LQ model,
N : total number of fractions,
d : dose per fraction,
T : overall treatment time,
T_d : effective tumor doubling time.

2.A. Optimization models and solution methods

A classic fractionation schedule optimization model in Problem (1) was extended to the 3D voxel-by-voxel formulation in Ref. 8. The input of this formulation is a fluence map (U) obtained from any conventional IMRT optimization prescribing a total prescription dose D in N_{conv} fractions. Let k^m be the total number of voxels in OAR m, and $\gamma(N)$ denote

the tumor repopulation term associated with N fractions such that

$$\gamma(N) = \ln 2 \frac{[T(N) - T_k]_+}{T_d}, \tag{2}$$

where $[\cdot]_+$ denotes $\max(0, \cdot)$. For the brevity of the notations, we also define several auxiliary parameters as follows:

$$s_j^m = \frac{A_j^m U}{D}, \tag{3}$$

$$\rho^m = \frac{1}{(\alpha^{\phi_m}/\beta^{\phi_m})}, \tag{4}$$

$$s_{\max}^m = \max_j s_j^m, j = 1,2,\ldots,k^m, \tag{5}$$

$$p^m = \sum_j^{k^m} s_j^m, \tag{6}$$

$$q^m = \sum_j^{k^m} (s_j^m)^2, \tag{7}$$

$$s_{\text{mean}}^m = q^m / p^m, \tag{8}$$

$$B_{\text{mean}}^m = q^m k^m \text{BED}_{\text{mean}}^m / (p^m)^2, \tag{9}$$

$$s_{\text{DVH}}^m = s_j^m, j \in J, \tag{10}$$

where A^m is a dose deposition coefficient matrix for OAR m so that A_{ij}^m is the dose deposited to voxel j in OAR m from beamlet i with unit intensity, i.e., $A_j^m U$ is the dose to voxel j in OAR m using a fluence map U.

Then, the fractionation schedule optimization using a full 3D voxel-by-voxel dose distribution can be written as

$$\max_{N, d_n} \alpha^\tau \sum_{n=1}^N d_n + \beta^\tau \sum_{n=1}^N d_n^2 - \gamma(N) \tag{11}$$

subject to

$$\sum_{n=1}^N (s_{\max}^m d_n) + \rho^m \sum_{n=1}^N (s_{\max}^m d_n)^2 \le \text{BED}_{\max}^m, m \in M_{\max}, \tag{12}$$

$$\sum_{n=1}^N (s_{\text{mean}}^m d_n) + \rho^m \sum_{n=1}^N (s_{\text{mean}}^m d_n)^2 \le \text{B}_{\text{mean}}^m, m \in M_{\text{mean}}, \tag{13}$$

$$\sum_{n=1}^N (s_{\text{DVH}}^m d_n) + \rho^m \sum_{n=1}^N (s_{\text{DVH}}^m d_n)^2 \le \text{BED}_{\text{DVH}}^m, m \in M_{\text{DVH}}, \tag{14}$$

$$d_n \ge 0, n = 1,2,\ldots,N, \text{ and } N \ge 1, \text{ integer},$$

where M_X and BED_X^m with $X \in \{\text{max, mean, DVH}\}$ are a set of OAR indices and tolerance BED known with a standard fractionation, i.e., D in N_{conv} fractions, for OAR m with X type of constraints, respectively. In this formulation, DVH constraints, which are discontinuous, were handled using the constraint generation method. This means that Problem (11) was first solved without the DVH constraint, i.e., $J = \{\}$. If the solution does not meet the DVH constraints, then Eq. (14) is added for the appropriate number of voxels that have violated the DVH constraints.

For fixed N, Problem (11) is nonconvex quadratically constrained quadratic programming (QCQP) in d because a convex function is maximized. Nonconvex QCQP is computationally challenging. However, it was proven in Ref. 8 that Problem (11) has an optimal, *stationary* solution if the tumor α/β ratio is greater than the maximum of all OAR α/β ratios or smaller than the minimum of all OAR α/β ratios. Since the lung tumor α/β ratio is often believed to be 10 Gy, which is larger than the α/β ratios of any OAR considered here, it satisfies the sufficient condition for the stationary solution. Furthermore, the quadratic constraints in Eqs. (12)–(14) can be equivalently written as linear constraints because $s_X^m d$ with $X \in \{\text{max, mean, DVH}\}$ is non-negative. Let M be a set of indices of all OARs. Then, Problem (11) with a stationary solution is reduced to

$$\max_N \alpha^\tau N d^*(N) + \beta^\tau N (d^*(N))^2 - \gamma(N) \tag{15}$$

subject to

$$d^*(N) = \min_{m \in M} \frac{-1 + \sqrt{1 + 4\rho^m C^m / N}}{2\sigma^m \rho^m},$$
$$N \ge 1, \text{ integer},$$

where σ^m and C^m are defined as the effective sparing factor (s_X^m) in the left hand side and tolerance BED in the right hand side of Eqs. (12)–(14). A heuristic search for N that maximizes the objective function in Eq. (15) is computationally inexpensive, and therefore used here.

2.B. Phantom selection and planning

Sixteen lung phantom cases were designed to represent clinically relevant anatomic conditions using in-house software, Phantom Creator (PhanC).[9] PhanC is a MATLAB (Ref. 10) code developed to create user-defined organs (e.g., tumor and OAR), beam coordinates, and a dose deposition coefficient matrix for IMRT fluence map optimization. Four different normal tissue geometries were constructed, and the distances among multiple OAR were manually sampled from clinical studies to best simulate clinical scenarios. For each normal tissue geometry, two different tumor locations were randomly selected to simulate various distances between a tumor and multiple OAR. Then, a tumor with two different sizes (a sphere shape with 5 and 7 cm diameter) was placed for each tumor location identified. Two sample cases are shown in Fig. 1. A dose deposition coefficient matrix was calculated without a heterogeneity correction.

Heart, lungs, cord, esophagus, and unspecified tissues were constrained to be under the tolerance of $D_{\text{mean}} \le 45$ Gy, $D_{\text{mean}} \le 20$ Gy, $D_{\max} \le 45$ Gy, $D_{\max} \le 63$ Gy, and $D_{05} \le 60$ Gy, respectively, if delivered in 30 fractions.[11] The standard fractionation (*base case*) was taken to be 60 Gy in 30 fractions. The fluence map was optimized using an in-house IMRT algorithm to deliver a uniform dose of 60 Gy to the tumor with hard constraints on all OARs, i.e., OAR dose must be under the tolerance level as specified above. The solution U to the standard spatial optimization was then used in the subsequent fractionation schedule optimization to find the optimal N^* without violating OAR BED constraints.

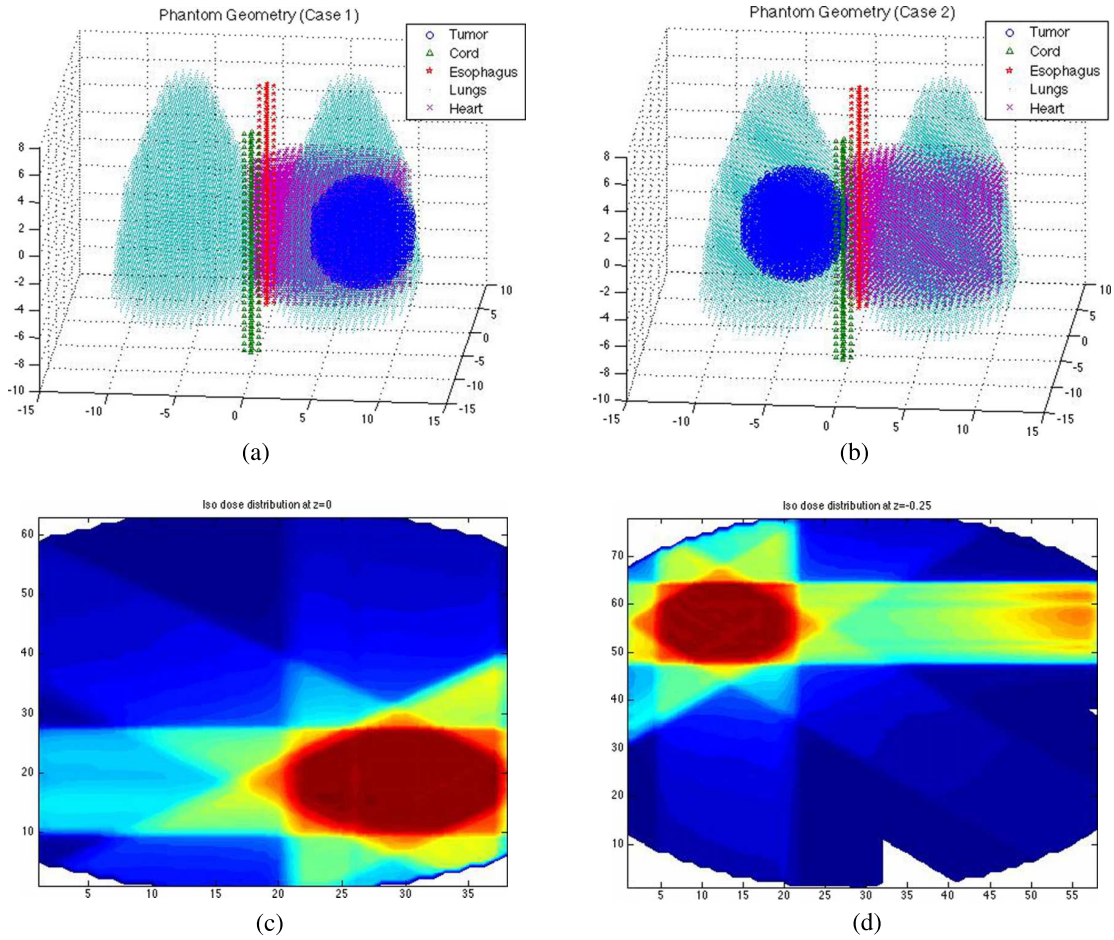

FIG. 1. Two phantom geometries are shown in (a) and (b). Transverse isodose distributions are shown for two different phantom cases in (c) and (d).

Each phantom case was planned using both a standard fractionation and an optimal fractionation schedule. The α/β ratio of 10 was used for the tumor and the α/β ratio of 3 was used for all OARs to consider late effects. Tumor doubling time (T_d) and lag time (T_k) were varied between 3–100 and 0–10 days, respectively. Dose calculations were done without a heterogeneity correction.

2.C. Evaluation criteria

It was proven in Ref. 8 that there is always a *finite* N^* that maximizes the objective function in Problem (15) regardless of the T_d used. However, the true maximum of the tumor BED may occur at a large value of N^* without a clinically significant gain in the tumor BED. Therefore, we define *practically optimal* values of N^*_{99}, N^*_{98}, and N^*_{95} for N^*, where 99%, 98%, and 95% of the true maximum of the tumor BED are achieved. Figure 2 shows an example of case 1 with two different α/β ratios for the tumor and $T_d = 10$ days. The maximum, minimum, mean, and D_{95} of the tumor BED were computed. All OAR doses are below the tolerance BED by design because they are hard-constrained, i.e., they must be under the tolerance doses. Therefore, they are not reported here.

In addition to tumor BED, we also computed the EUD. Let ρ_i and d_i be the tumor density and the dose in voxel i, respectively. Then, the fractional EUD (fEUD) is given by

$$\sum_{i=1}^{n} \rho_i \left(\exp\left[-\alpha(\text{fEUD})_i - \beta(\text{fEUD})_i^2\right]\right)^N = \sum_{i=1}^{n} \rho_i \left(\exp\left[-\alpha d_i - \beta d_i^2\right]\right)^N. \quad (16)$$

Since $\text{fEUD}_i = \text{fEUD}$ for all voxel i and $\text{fEUD} \times N = \text{EUD}$ after all fractions are delivered, Eq. (16) is reduced to

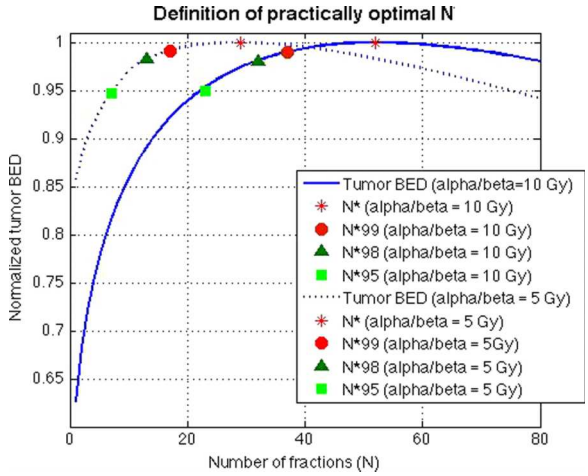

FIG. 2. Definition of *practically optimal* N^*_{95}, N^*_{98}, N^*_{99} which represent fractionation schedules that result in clinically similar tumor BEDs.

$$\exp\left[-\alpha \mathrm{EUD} - \beta \mathrm{EUD}^2/N\right] = \frac{\sum_{i=1}^{n} \rho_i \left(\exp\left[-\alpha d_i - \beta d_i^2\right]\right)^N}{\sum_{i=1}^{n} \rho_i}. \quad (17)$$

Assuming the uniform cell density ρ for all voxels, it is further reduced to

$$\mathrm{EUD} = \frac{N}{2}\left(\frac{\alpha}{\beta}\right) \times \left[-1 + \sqrt{1 + \frac{4}{N}\left(\frac{\beta}{\alpha^2}\right) \ln\left\{\frac{n}{\sum_{i=1}^{n}\left(\exp\left[-\alpha d_i - \beta d_i^2\right]\right)^N}\right\}}\right]. \quad (18)$$

The EUD is the uniform (physical) dose of radiation that kills the same number of tumor cells as a nonuniform (physical) dose distribution. As such, estimates of the EUD are directly comparable in magnitude to the prescribed (physical) tumor dose used in the base case. On the other hand, BED is a biological dose that is always greater than the prescription dose, except for the special case when $\alpha/\beta >> D$ (total treatment dose). BED allows for a direct comparison of treatment schemes with different fractionation schedules.

3. RESULTS

Tumor BED and EUD were not sensitive to the various tumor lag-times (T_k) used, i.e., 0–10 days, except that T_k set the lower bound on the optimal N^*, i.e., $N^* > T_k$, and this finding agrees with the previous studies.[8] For example, Table II shows an optimal N^* for various T_d with $T_k = 0$. Optimal N^* s are identical for all T_k except N^*_{95} with $T_k \geq 7$ days because an optimal N^* is larger than the maximum T_k used in the simulations, i.e., 10 days. When $T_k = 10$ days are used with $T_d = 3$ days, the optimal N^*_{95} is 11 fractions ($=T_k + 1$). Therefore, to avoid redundancy, all results are presented for $T_k = 0$ only.

We normalized the BED and EUD with an optimal fractionation schedule to those with the standard fractionation. Normalized BED and EUD we report here are given by

$$\text{Normalized optimal BED (EUD) in \%} = \frac{\text{BED (EUD) with an optimal fractionation}}{\text{BED (EUD) with a standard fractionation}} \times 100.$$

As T_d increases, the gain in tumor BED increases, as does N^*. The optimal tumor max, min, mean, and D_{95} BED are 102.2%–118.5%, 102.0%–119.8%, 102.2%–118.9%, and 102.1%–119.3% of the corresponding values with the standard fractionation (base case). The optimal N^* averaged over all 16 phantom cases ranges from 17 to 249 fractions depending on the T_d used. Practically optimal N^*_{99}, N^*_{98}, and N^*_{95} range from 12, 10, and 7 to 157, 128, and 84 fractions (see Fig. 2 for a graphical description of N^*). As tumor α/β ratios decrease, the values of N^*, N^*_{99}, N^*_{98}, and N^*_{95} also decrease. Their corresponding max, min, mean, and D_{95} BED are 101.2%–117.3%, 101.2%–118.7%, 101.2%–117.8%, and 101.2%–118.2% for N^*_{99}, 100.3%–116.1%, 100.3%–117.5%, 100.3%–116.6%, and 101.2%–117.0% for N^*_{98}, and 97.5%–112.7%, 97.4%–113.8%, 97.4%–113.1%, and 97.4%–113.4% for N^*_{95}. Table I summarizes the optimal BED normalized to the BED with the standard fractionation.

The corresponding optimal N^*, N^*_{99}, N^*_{98}, and N^*_{95} are presented in Table II. We computed the corresponding total physical mean dose delivered to the tumor with optimal N^*, N^*_{99}, N^*_{98}, and N^*_{95}. The average mean dose to the tumor

TABLE I. Normalized optimal BED averaged over all 16 phantom cases with $T_k = 0$ (tumor BED with the standard fractionation = 100 %). The different columns represent the change using spatiotemporal optimization in the tumor metrics (max, min, mean, D_{95}) relative to standard fractionation for the optimal (N^*) and each of the *practically optimal* (N^*_{99}, N^*_{98}, N^*_{95}) fractionations.

T_d (days)	Tumor BED	N^*	N^*_{99}	N^*_{98}	N^*_{95}
3	Max (%)	103.8	102.9	101.8	98.9
	Min	106.0	105.4	104.4	101.4
	Mean	104.4	103.5	102.4	99.5
	D_{95}	104.9	104.2	103.1	100.1
10	Max	102.2	101.2	100.3	97.5
	Min	102.0	101.2	100.3	97.4
	Mean	102.2	101.2	100.3	97.4
	D_{95}	102.1	101.2	100.3	97.4
20	Max	107.2	106.1	105.1	102.0
	Min	107.3	106.4	105.4	102.1
	Mean	107.3	106.2	105.2	102.0
	D_{95}	107.3	106.3	105.3	102.0
30	Max	110.3	109.2	108.2	105.0
	Min	110.7	109.8	108.7	105.4
	Mean	110.5	109.4	108.4	105.1
	D_{95}	110.6	109.5	108.5	105.2
60	Max	115.3	114.2	113.0	109.7
	Min	116.3	115.2	114.1	110.5
	Mean	115.6	114.5	113.4	109.9
	D_{95}	115.9	114.8	113.7	110.2
100	Max	118.5	117.3	116.1	112.7
	Min	119.8	118.7	117.5	113.8
	Mean	118.9	117.8	116.6	113.1
	D_{95}	119.3	118.2	117.0	113.4

TABLE II. Optimal number of fractions averaged over all 16 phantom cases ($T_k = 0$). The range of the optimal N^*, N^*_{99}, N^*_{98}, and N^*_{95} for 16 cases is shown inside the parenthesis.

T_d (days)	N^*	N^*_{99}	N^*_{98}	N^*_{95}
3	17	12	10	7
5	28	20	17	12
10	51 (43–52)	36 (30–37)	31 (27–32)	23 (20–23)
20	87 (72–89)	60 (49–62)	52 (41–53)	36 (29–37)
30	116 (96–119)	79 (64–81)	67 (53–69)	47 (36–48)
60	183 (151–187)	120 (95–123)	99 (78–102)	67 (51–69)
100	249 (205–256)	157 (125–162)	128 (100–132)	84 (64–87)

TABLE III. Optimal (physical) total mean dose to the tumor in Gy ($T_k = 0$) averaged over 16 cases with N^*, N^*_{99}, N^*_{98}, and N^*_{95} fractions. The range of the optimal total mean dose to the tumor in 16 cases is shown inside the parenthesis.

T_d (days)	N^*	N^*_{99}	N^*_{98}	N^*_{95}
3	50.2 (48.9–50.5)	44.8 (44.4–45.0)	42.0 (41.6–42.1)	36.8 (36.5–36.9)
5	58.5 (58.0–58.8)	53.0 (52.5–53.2)	50.3 (49.9–50.5)	44.8 (44.4–45.0)
10	67.9 (65.0–68.7)	62.6 (59.7–63.3)	60.3 (58.0–61.0)	55.0 (53.1–55.5)
20	75.5 (71.7–76.4)	70.5 (66.8–71.4)	68.1 (64.3–69.0)	62.5 (59.2–63.3)
30	79.0 (74.9–80.0)	74.2 (70.2–75.2)	71.9 (67.8–71.9)	66.5 (62.4–67.5)
60	83.4 (79.2–84.7)	79.3 (74.8–80.4)	77.1 (72.6–78.2)	71.9 (67.3–72.9)
100	86.2 (81.5–87.4)	82.2 (77.5–83.4)	80.1 (75.4–81.2)	75.0 (70.2–76.1)

and its range in Gy for 16 cases are summarized in Table III. The average mean dose to the tumor using the standard fractionation for 16 cases ranged from 59.1 to 59.9 Gy with the average of 59.6 Gy.

The optimal tumor EUD averaged over 16 cases was 100%–117.0%, 99.4%–116.2%, 98.7%–115.1%, and 96.5%–111.8% of the EUD with the standard fractionation depending on N^*, N^*_{99}, N^*_{98}, and N^*_{95}. Normalized optimal tumor EUD is shown in Table IV.

We also compared the impact of the tumor size on the tumor BED with an optimal fractionation normalized to those with the standard fractionation. The results are summarized in Table V and the p-value is shown for the two sets of plans: one set with eight large tumors and the other set with eight small tumors. Note that the small tumors have a larger distance from OAR than the large tumors because they share the same isocenter and OAR geometries.

4. DISCUSSION

Historically, the standard fractionation scheme (daily for 4–8 weeks) has been used to give the normal tissues time to repair from radiation damage between fractions. However, the advances made in dose localization, i.e., IMRT and image-guided radiation therapy (IGRT), allow for much less dose to OAR for a given tumor dose than 3D conformal radiation therapy (3DCRT), thereby allowing a reduction in the normal tissue toxicity even with a short treatment course and a larger fractional dose. These advances led to the development of SBRT, which utilizes fewer fractions (3–5) with a larger dose per fraction. Multiple studies indicate that the success of nonconventional RT, including SBRT for early stage, inoperable lung cancer patients, is highly correlated with the larger BED delivered to the tumor.[12–25] Some of the nonconventional fractionation schedules have been empirically tried (RTOG 1005, 9512, 9003) and the optimal fractionation schedule is yet unknown.

It has repeatedly been found in many previous studies with the stylistic model as in Problem (1) that the key components in determining an optimal fractionation schedule are (a) tissue-specific radiosensitivity parametrized by α and β, (b) tumor-specific T_d and T_k, and (c) the relative dose received by the tumor and multiple OARs. Since these values vary greatly among patients, the purpose of this study was to investigate the feasibility of selecting a fractionation schedule based on the specific patient geometry, and to quantify the potential dosimetric benefits. One of the main findings of this current work is that when the fractionation schedule optimization model was fully extended to the 3D voxel-by-voxel dose distribution, it was possible to incorporate the realistic dose relationship among tumor and multiple OARs. This also enables the planners to use three types of constraints (max, mean, and DVH) for OAR that are routinely used in current practice to evaluate treatment plans.

Results of the phantom studies suggest that personalizing a fractionation schedule could potentially deliver a larger BED

TABLE IV. Normalized optimal tumor EUD with $T_k = 0$ in percentage, averaged over all 16 cases (tumor EUD with the standard fractionation = 100%).

T_d (days)	N^*	N^*_{99}	N^*_{98}	N^*_{95}
3	103.1	102.6	101.9	99.8
5	100	99.4	98.7	96.5
10	101.7	101	100.2	98.0
20	105.9	105.1	104.3	101.7
30	108.8	108.0	107.1	104.4
60	113.7	112.9	111.9	108.8
100	117.0	116.2	115.1	111.8

TABLE V. The range of normalized, optimal tumor max, min, mean, and D_{95} BED in percentage for eight small tumors with 5 cm diameter and eight large tumors with 7 cm diameter. The results are shown with $T_d = 100$ and $T_k = 0$.

Tumor BED	Tumor size	N^*	N^*_{99}	N^*_{98}	N^*_{95}
Max	Small	124.7–125.5	121.1–121.8	119.2–119.8	114.6–115.0
	Large	117.4–125.1	114.2–121.4	112.5–119.5	108.4–114.8
	p-value	0.070	0.069	0.071	0.073
Min	Small	126.4–127.5	122.5–123.5	120.5–121.4	115.6–116.3
	Large	119.7–128.7	116.2–124.5	114.2–122.3	108.4–117.0
	p-value	0.199	0.183	0.175	0.154
Mean	Small	125.8–125.9	122.0–122.1	120.0–120.1	115.2–115.3
	Large	118.2–125.9	114.9–122.0	113.1–120.1	108.8–115.3
	p-value	0.083	0.081	0.082	0.082
D_{95}	Small	126.0–126.9	122.3–123.0	120.2–120.9	115.4–115.9
	Large	118.7–126.7	115.3–122.8	113.4–120.7	109.0–115.8
	p-value	0.083	0.081	0.082	0.083

and EUD to tumors without exceeding the normal tissue BED tolerance dose levels currently assumed to be safe for the tumors with a large T_d. On the other hand, for the fast growing tumors with a small T_d, there is no significant difference in tumor BED between an optimal fractionation and a standard fractionation. However, the optimal number of fractions found was smaller than the standard number of fractions. Although there is no dosimetric gain, a shorter treatment course would increase the convenience of the patients and provides the facility with a more efficient allocation of the resources. The results also showed that an optimal N^* does not depend on T_k as long as N^* is larger than T_k. Intuitively, T_k plays an insignificant role because (i) $\gamma(N)$ is strictly positive only when T_k is less than the number of fractions, i.e., $T(N)$, as seen in Eq. (2) and (ii) the magnitude of $\gamma(N)$ becomes significant only when $T_k \gg T_d$.

The comparison of the improvement in the tumor BED using an optimal fractionation over the standard fractionation between small and large tumors shows that a larger BED could be delivered to a smaller tumor, i.e., a larger distance between the tumor and OAR in our test cases for given normal tissue tolerance doses. This means that the benefit of using an optimal fractionation scheme, instead of the standard fractionation, will be larger for the patients with smaller tumors. This finding is in line with the current practice of SBRT, where smaller tumors are treated with a nonconventional, hypofractionation scheme. Currently, there are rather strict limits on the eligibility of patients for SBRT treatments given the difficulty in performing the exhaustive clinical trials needed to explore the large range of tumor positions and sizes, and the possible fractionation schemes. The methods described in this paper may be used (i) to determine if a given patient would benefit from an SBRT-like regimen, i.e., higher than conventional daily dose ($\geq$1.8–2.0 Gy) and fewer fractions ($\leq$30–35 fx) and (ii) to help design clinical studies to classify tumor characteristics and appropriate fractionation schedules. For example, the spatiotemporal optimization may identify a feasible SBRT-like fractionation scheme for the patients with larger tumors that are currently excluded from the current SBRT protocol because they have a favorable geometry.

If one is interested in sparing normal tissues rather than increasing tumor BED for a higher tumor control, an optimal fractionation schedule also offers the opportunity to achieve this goal. Using the optimal number of fractions found, an optimized plan can be easily scaled down in the fluence map to match the current tumor BED. Then, a smaller OAR BED would be delivered for the same tumor BED as the standard fractionation scheme.

On a practical note, considering the uncertainty inherent in any biological parameters and a wide range of tumor doubling times previously reported, e.g., 30–490,[26] 8–171,[27] and 32–26 711 days,[28] a *threshold* could be employed to define the tumor doubling time as "large" or "small" instead of a specific value for T_d. For example, in most clinic settings with IGRT capability, the patients who undergo radiotherapy have a waiting period between simulation and the first treatment; therefore, two CT datasets (planning CT and cone-beam CT) are available without additional cost to estimate whether the patient-specific T_d is below or above the threshold. Alternatively, if there is a diagnostic CT scan available, then this could also be used with a treatment planning CT without additional cost to estimate T_d. Utilizing functional imaging modalities may also provide a useful method for estimating T_d value.

5. LIMITATIONS OF THIS STUDY AND FUTURE WORK

Optimal fractionation schedule is dependent on the patient variability in their geometry and radiobiological parameters. This study investigated the feasibility of selecting a patient-specific fractionation schedule to deliver a larger tumor BED without increasing BED to OAR (or equivalently to decrease BED to OAR without decreasing BED to the tumor) using phantom cases. Additional research using patient CT datasets and heterogeneity corrections in the dose calculation is needed to better assess the difference in dose between a tumor and OAR, and therefore an optimal, personalized fractionation schedule to be recommended for clinical trials. Using a fluence map from SBRT plans rather than a conventional plan as used in this study will highlight the dosimetric gains with an optimal fractionation schedule because SBRT plans tend to have a larger difference between a tumor dose and OAR dose. Investigation on the SBRT-like fractionation scheme for the intermediate size of tumors is also encouraged. Finally, incorporating patient-specific biological information (α,β,T_d,T_k), if available through functional imaging, will lead to a more optimal, personalized treatment schedule. Performing sensitivity analyses on these parameters may determine the range over which spatiotemporal optimization may prove beneficial.

[a]Electronic mail: mk688@uw.edu

[1]J. F. Fowler, "How worthwhile are short schedules in radiotherapy?: A series of exploratory calculations," Radiother. Oncol. **18**, 165–181 (1990).
[2]J. F. Fowler and M. A. Ritter, "A rationale for fractionation for slowly proliferating tumors such as prostatic adenocarcinoma," Int. J. Radiat. Oncol., Biol., Phys. **32**, 521–529 (1995).
[3]Y. Yang and L. Xing, "Optimization of radiotherapy dose-time fractionation with consideration of tumor specific biology," Med. Phys. **12**, 3666–3677 (2005).
[4]A. Bertuzzi, C. Bruni, F. Papa, and C. Sinisgalli, "Optimal solution for a cancer radiotherapy problem," J. Math. Biol. **1-2**, 311–349 (2013).
[5]M. Mizuta, S. Takao, H. Date, N. Kishimoto, K. L. Sutherland, R. Onimaru, and H. Shirato, "A mathematical study to select fractionation regimen based on physical dose distribution and the linear-quadratic model," Int. J. Radiat. Oncol., Biol., Phys. **84**, 829–833 (2012).
[6]J. Unkelbach, D. Craft, E. Saleri, J. Ramakrishnan, and T. Bortfeld, "The dependence of optimal fractionation schemes on the spatial dose distribution," Phys. Med. Biol. **1**, 159–167 (2013).
[7]T. Bortfeld, J. Ramakrishnan, J. N. Tsitsiklis, and J. Unkelback, "Optimization of radiotherapy fractionation schedules in the presence of tumor repopulation," e-print arXiv:1312.1332 (2013).
[8]F. Saberian, A. Ghate, and M. Kim, "Optimal fractionation in radiotherapy with multiple normal tissues," Math. Med. Biol. (published online).
[9]F. Saberian and M. Kim, Phantom Creator (PhanC): A MATLAB software for creating phantom test cases for IMRT optimization, user manual available, University of Washington, 2014.
[10]MathWorks, Natick, MA.
[11]L. B. Marks, E. D. Yorke, A. Jackson, R. K. T. Haken, L. S. Constine, A. Eisbruch, S. M. Bentzen, J. Nam, and J. O. Deasy, "Use of normal tissue complication probability models in the clinic," Int. J. Radiat. Oncol., Biol., Phys. **76**, S10–S19 (2010).

[12]J. Seong *et al.*, "A multicenter retrospective cohort study of practice patterns and clinical outcome on radiotherapy for hepatocellular carcinoma in Korea," Liver Int. **29**, 147–152 (2009).
[13]J. Boda-Heggemann *et al.*, "Clinical outcome of hypofractionated breath-hold image-guided SABR of primary lung tumors and lung metastases," Radiat. Oncol. **9**, 10 (2014).
[14]A. Mandal, A. Asthana, and L. Aggarwal, "Clinical significance of cumulative biological effective dose and overall treatment time in the treatment of carcinoma cervix," Med. Phys. **32**, 68–72 (2007).
[15]B. Xia *et al.*, "The effect of bioequivalent radiation dose on survival of patients with limited-stage small-cell lung cancer," Radiat. Oncol. **6**, 50 (2011).
[16]A. Chi, Z. Liao, N. Nguyen, J. Xu, B. Stea, and R. Komaki, "Systemic review of the patterns of failure following stereotactic body radiation therapy in early-stage non-small-cell lung cancer: Clinical implications," Radiother. Oncol. **94**, 1–11 (2010).
[17]D. Rades, V. Rudat, T. Veninga, L. Stalpers, P. Hoskin, and S. Schild, "Prognostic factors for functional outcome and survival after reirradiation for in-field recurrences of metastatic spinal cord compression," Cancer **113**, 1090–1096 (2008).
[18]R. Yoshimura *et al.*, "Radiotherapy doses at special reference points correlate with the outcome of cervical cancer therapy," Brachytherapy **7**, 260–266 (2008).
[19]J. Brown, D. Brenner, and D. Carlson, "Dose escalation, not 'new biology,' can account for the efficacy of stereotactic body radiation therapy with non-small cell lung cancer," Int. J. Radiat. Oncol., Biol., Phys. **85**, 1159–1160 (2013).
[20]J. Brown, D. Carlson, and D. Brenner, "The tumor radiobiology of SRS and SBRT: Are more than the 5 Rs involved?," Int. J. Radiat. Oncol., Biol., Phys. **88**, 254–262 (2014).
[21]L. Kestin, I. Grills, M. Guckenberger, J. Belderbos, A. Hope, M. Werner-Wasik, J. Sonke, J. Bissonnette, Y. Xiao, D. Yan, and E. L. R. Group, "Dose–response relationship with clinical outcome for lung stereotactic radiotherapy delivered via online image guidance, radiotherapy oncology," Radiother. Oncol. **110**, 499–504 (2014).
[22]T. Yamamoto, K. Jingu, Y. Shirata, M. Koto, H. Matsushita, T. Sugawara, M. Kubozono, R. Umezawa, K. Abe, N. Kadoya, Y. Ishikawa, M. Kozumi, N. Takahashi, K. Takeda, and Y. Takai, "Outcomes after stereotactic body radiotherapy for lung tumors, with emphasis on comparison of primary lung cancer and metastatic lung tumors," BMC Cancer **14**, 464 (2014).
[23]S. Park, S. Urm, and H. Cho, "Analysis of biologically equivalent dose of stereotactic body radiotherapy for primary and metastatic lung tumors," Cancer Res. Treat. **46**, 403–410 (2014).
[24]M. Guckenberger, M. Allgäuer, S. Appold, K. Dieckmann, I. Ernst, U. Ganswindt, R. Holy, U. Nestle, M. Nevinny-Stickel, S. Semrau, F. Sterzing, A. Wittig, and N. Andratschke, "Safety and efficiency of stereotactic body radiotherapy for stage I non-small-cell lung cancer in routine clinical practice: A patterns-of-care and outcome analysis," J. Thorac. Oncol. **8**, 1050–1058 (2013).
[25]H. Onishi, H. Shirato, Y. Nagata, M. Hiraoka, M. Fujino, K. Gomi, Y. Niibe, K. Karasawa, K. Hayakawa, Y. Takai, T. Kimura, A. Takeda, A. Ouchi, M. Hareyama, M. Kokubo, R. Hara, J. Itami, K. Yamada, and T. Araki, "Hypofractionated stereotactic radiotherapy for stage I non-small cell lung cancer: Updated results of 257 patients in a Japanese multi-institutional study," J. Thorac. Oncol. **7**, S94–S100 (2007).
[26]J. Steele and P. Buell, "Asymptomatic solitary pulmonary nodules: Host survival, tumor size, and growth rate," J. Thorac. Cardiovasc. Surg. **65**, 140–151 (1973).
[27]S. E. Sharouni, H. Kal, and J. Battermann, "Accelerated regrowth of non-small-cell lung tumours after induction chemotherapy," Br. J. Cancer **89**, 2184–2189 (2003).
[28]S. Jennings, H. Winer-Muram, M. Tann, J. Ying, and I. Dowdeswell, "Distribution of stage I lung cancer growth rates determined with serial volumetric CT measurements," Radiology **241**, 554–563 (2006).